Stress fluctuations and motion of cytoskeletal-bound markers

Carina Raupach,[1] Daniel Paranhos Zitterbart,[1] Claudia T. Mierke,[1] Claus Metzner,[1] Frank A. Müller,[2] and Ben Fabry[1,*]
[1]*Center for Medical Physics and Technology, Biophysics Group, University of Erlangen-Nuremberg, 91052 Erlangen, Germany*
[2]*Department of Materials Science-Biomaterials, University of Erlangen-Nuremberg, 91052 Erlangen, Germany*
(Received 22 December 2006; published 25 July 2007)

Cytoskeletal (CSK) dynamics such as remodeling and reorganization can be studied by tracking the spontaneous motion of CSK-bound particles. Particle motion is thought to be driven by local, ATP-dependent intracellular force fluctuations due to polymerization processes and motor proteins, and to be impeded by a viscoelastic, metastable cytoskeletal network. The mechanisms that link particle motion to force fluctuations and the CSK dynamics remain unclear. We report simultaneous measurements of the spontaneous motion of CSK-bound particles and of cellular force fluctuations. Cellular force fluctuations were measured by tracking fluorescent markers embedded in an elastic polyacrylamide hydrogel substrate that served as an extracellular matrix (ECM). The motion of CSK-bound particles and markers embedded in the ECM showed both persistence and superdiffusive behavior. Moreover, the movements of CSK-bound beads were temporally and spatially correlated with force fluctuations in the ECM. The findings suggest that the spontaneous motion of CSK-bound beads is driven not by random, local stress fluctuations within a viscoelastic continuum or cage, but rather by stress fluctuations within a tensed and constantly remodeling CSK network that transmits stresses over considerable distances to the ECM.

DOI: 10.1103/PhysRevE.76.011918 PACS number(s): 87.15.Ya, 87.17.Jj, 87.15.Vv, 87.16.Ka

I. INTRODUCTION

A number of essential activities of living cells rely on fine-tuned mechanical events that involve force generation and shape changes. Examples of such activities include intracellular transport, cell crawling, cell spreading, and cell division. The structural basis of these mechanical events are filamentous scaffolding proteins called cytoskeletal (CSK) filaments (such as filamentous actin and microtubules) and motor proteins (such as myosins or kinesins) that connect to and move along the CSK filaments. The CSK alone, without motor proteins, can also move and generate forces; it is a highly dynamic structure in a continuous state of disassembly and reassembly [1,2].

The dynamic reorganization of the CSK has attracted considerable interest because it is such a crucial component of cell behavior. To quantify CSK dynamics in living cells, a number of techniques has been developed, such as fluorescence recovery after photobleaching (FRAP) and fluorescence speckle microscopy [3]. The principal idea behind these techniques is to mark a small component of the CSK (by photobleaching or fluorescent labeling) and to follow its movements, recovery, or disappearance. A related technique is nanoscale particle tracking, where a large particle (of the order of 1 μm) is bound to the CSK [4–6]. Because of its large size, spatial movements can be followed with nanometer precision. Depending on surface functionalization, such large particles can form multiple bonds with the CSK. The particles can move spontaneously if the CSK structure to which they are attached undergoes rearrangements [4,6–8]. Consequently, bead movements as quantified by their mean-square displacement (MSD) would report the rate of ongoing CSK rearrangements over time [6]. Another possible source of bead movements are force fluctuations (force hits onto the bead) due to the action of motor proteins that cause deformations of the viscoelastic medium surrounding the bead [5,9]. A third contributing mechanism is the motion of the bead in a cage formed by the surrounding CSK mesh that allows the occasional hopping of the bead out of its cage [5,10,11].

While the mechanical coupling of CSK-bound beads to the CSK has been relatively well studied using optical tweezers, magnetic tweezers, and magnetic twisting cytometry [12–16], the cellular forces that move the beads in the absence of external force are not well understood. The aim of this study was to investigate the forces that drive spontaneous bead motion. By plating the cells onto flexible, elastic polyacrylamide gels that served as an extracellular matrix (ECM) and measuring the gel deformation from the displacements of gel-embedded fluorescent beads, the tractions that the cells exert on the ECM can be inferred [17–19]. In addition, the spontaneous motion of fibronectin-coated beads bound to the CSK via integrin receptors on the apical surface of the cells was measured. Statistical measures of the motion of the CSK-bound and ECM-bound beads were then compared. For time lags between 5 and 100 s, ECM- and CSK-bound beads displayed similar superdiffusive and persistent motion. Persistence and superdiffusivity of both CSK- and ECM-bound particles showed large, synchronous fluctuations over time that were highly correlated. Moreover, the movements of CSK-bound beads were spatially correlated with force fluctuations in the ECM. The findings are consistent with the notion that the spontaneous motion of CSK-bound beads is driven by large-scale stress fluctuations within a tensed, continuously remodeling CSK network that transmits stresses over considerable distances to the ECM.

*Corresponding author. FAX: +49 9131 85 25601. bfabry@biomed.uni-erlangen.de

II. MATERIALS AND METHODS

A. Cell culture

Mewo skin and MDA-MB-231 breast carcinoma cells were cultured in Dulbecco's modified Eagle's medium (DMEM with 1 g/l glucose) supplemented with 10% fetal calf serum, 2 mM L-glutamine, and 100 U/ml penicillin-streptomycin at 37 °C in humidified air containing 5% CO_2. Twenty-four to 72 hours prior to the measurements, adherent cells were harvested with Accutase (PAA Laboratories, Linz, Austria), and 400 000 cells were plated in 35-mm-diameter culture dishes (Nunclon Surface) and cultured in DMEM at 5% CO_2 and 37 °C.

Human endothelial cells were isolated from the vein of umbilical cords (HUVEC). The vein was washed with PBS buffer, and the endothelial cells were isolated using trypsin/EDTA (0.25%/0.2%) solution. Endothelial cells were maintained in Endothelial Cell Growth Medium 2 (Promocell, Heidelberg, Germany). The cells were harvested using Accutase, and 400 000 cells were plated on polyacrylamide gels and grown overnight to confluence in Endothelial Cell Growth Medium 2 at 5% CO_2 and 37 °C.

B. Beads

Here 4.5-μm epoxylated polystyrene beads (Dynal M-450 Epoxy, Oslo, Norway) or 1-μm carboxylated fluorescent polystyrene beads (Molecular Probes, Eugene, OR) were coated with human fibronectin (100 μg/ml per 4×10^9 beads) (Roche Applied Science, Cat No. 688851) in PBS at 4 °C for 24 h. Beads were washed twice in PBS and stored at 4 °C. Prior to measurements, beads were sonicated, added to the cells (2×10^5 beads/dish), and incubated for 30 min at 5% CO_2 and 37 °C. Measurements were performed in an incubator mounted on the microscope stage at 5% CO_2 and 37 °C.

C. Fluorescence microscopy

Fluorescent images were recorded at a maximum rate of 8.3 images per second with a charge-coupled device (CCD) camera (Hamamatsu Orca-ER) mounted on an inverted microscope equipped with a 10×, 0.3 NA or a 20×, 0.4 NA objective. The microscope was placed on a vibration isolation table (Newport, Irvine, CA).

D. Spontaneous bead movements

Bead positions of typically 50–200 beads per field of view were tracked continuously for 5–40 min by computing the intensity-weighted average (center of mass) of each bead [accuracy 10 nm (rms) for 10× magnification of the objective and 5 nm (rms) for 20× magnification] [20]. Bead positions were corrected for the effects of microscope stage drift. The stage drift was estimated from changes in the mean position of reference beads within a field of view [6]. We computed the MSD for each bead as

$$\langle \Delta r^2(\Delta t)\rangle = \langle [\vec{r}(t+\Delta t)-\vec{r}(t)]^2\rangle, \tag{1}$$

where $\vec{r}$ is the position of the bead, Δt is the time lag, and $\langle\cdots\rangle$ brackets indicate the time average. A three-parameter equation

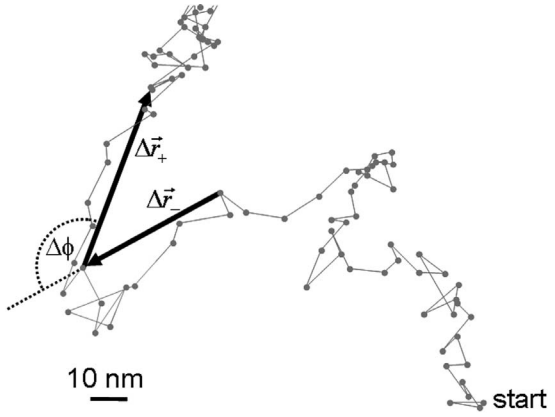

FIG. 1. Measurement of the turning angles $\Delta\phi(t,\Delta t)$ of the bead trajectory from a Mewo skin carcinoma cell. The bead positions are sampled every 120 ms (indicated by dots). This example shows $\Delta\phi$ for t=5.4 s, Δt=1200 ms.

$$\langle \Delta r_{\mathrm{fit}}^2(\Delta t)\rangle = c + D(\Delta t/t_0)^{\beta} \tag{2}$$

was fit to the MSD data of each bead by minimizing the squared differences between the logarithm of the data and the logarithm of the fit equation, summed over all Δt. t_0 was set arbitrarily to 1 s, and the fit parameters c and D were expressed in units of nm^2. Depending on the power-law exponent β, the bead motion can be classified as Brownian or diffusive for β=1, subdiffusive for $\beta<1$, superdiffusive for $\beta>1$, and ballistic for β=2 [5–7,9,10].

Equation (2) is an empirical relationship solely for the purpose of describing the MSD of individual beads with a minimum set of parameters. Equation (2) is not intended to predict the behavior outside the measurement range or to suggest that the superdiffusive part of the MSD is time-scale free or that the subdiffusive part of the MSD exhibits a plateau at small Δt.

E. Turning angle

To quantify directional changes in the bead motion, turning angles $\Delta\phi(t,\Delta t)$ in the bead trajectory $\vec{r}(t)$ between two successive trajectory segments of duration Δt were computed (Fig. 1):

$$\Delta\phi(t,\Delta t) = \angle\,(\Delta\vec{r}_+,\Delta\vec{r}_-), \quad \Delta\phi\in[-\pi,\pi),$$

with

$$\Delta\vec{r}_- = \vec{r}(t)-\vec{r}(t-\Delta t), \quad \Delta\vec{r}_+ = \vec{r}(t+\Delta t)-\vec{r}(t).$$

F. Traction microscopy

Gels for traction experiments were cast on rectangular 75×25 mm nonelectrostatic silane-coated glass slides (Menzel, Braunschweig, Germany) according to the procedure described by Pelham and Wang [19]. Gels with 6.1% acrylamide and 0.24% bis-acrylamide were used. The Young's modulus of the gels was measured with a magnetically driven plate rheometer and found to be 13 kPa [21]. Yellow-green fluorescent 0.5-μm carboxylated beads (Molecular

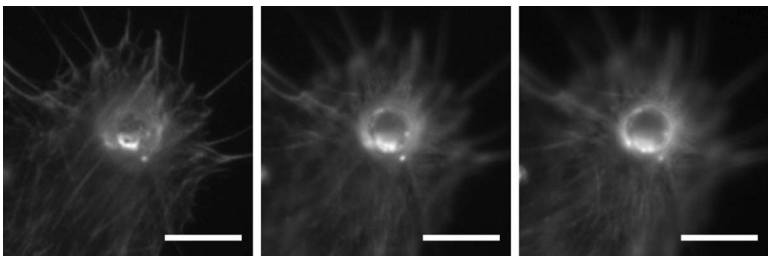

FIG. 2. A fibronectin-coated microbead bound to the actin cytoskeleton (stained with phalloidin) of an endothelial cell. A dense web of actin fibers surrounds the bead. Images were recorded at different focal planes 2 μm apart. Bars 10 μm.

Probes, Eugene, OR) were suspended in the gels and centrifuged at 300 g towards the gel surface during polymerization at 4 °C. The beads served as markers for gel deformations. The surface of the gel was activated with sulfo-SANPAH (Pierce Biotechnology) and coated with bovine collagen G (Biochrom, Berlin, Germany) at 50 μg/ml. The cell suspension added to the gel was contained in a silicone ring (flexiperm, In Vitro, Göttingen, Germany) attached to the glass slide. Cell tractions were computed from the displacement field of the gel surface [17].

G. Estimating the displacement field from the images

To estimate the displacement field of the gel surface, digital images taken every 0.23 s of the same gel region were compared. The bead density at the gel surface was approximately 50 000 beads within a field of view of 330 $\times$433 μm^2 (1024$\times$1344 pixels). Each bead image occupied an area of $\sim$3 pixels in diameter, and neighboring beads were usually less than 8 pixels apart. The image was divided into small segments (windows) with a size of 11$\times$11 pixels to guarantee that the window contained at least one fluorescent marker. In what follows, the phrase "bead in the gel" is short for "a square region at the gel surface spanning 11 $\times$11 pixels (3.5$\times$3.5 μm^2)". Gel deformations were computed by comparing two corresponding windows from a pair of images (i.e., windows with the same spatial coordinates). A simple cross-correlation method was used to obtain the gel deformations in integer units of the pixel spacing (322 nm/pixels). Gel deformations with subpixel resolution were then obtained using a difference-with-interpolation method [22]: Each 11$\times$11 pixel window of the second image was shifted by a subpixel value, and then the mean-square difference of the intensity values was calculated between the shifted window and the corresponding 11$\times$11 pixels window from the first image. This procedure was repeated with different subpixel shift values until a minimum of the mean-square differences was found. To speed up the process, the subpixel shift was limited to integer multiples of 1/40 of a pixel (corresponding to 8 nm). The subpixel shift was done with a Fourier interpolation method: The image window to be shifted was transformed into the Fourier domain and multiplied by $\exp(i2\pi\vec{r})$, where $i=\sqrt{-1}$ and $\vec{r}$ denotes the translational shift. Because of the wraparound of pixels that are shifted outside the window, the window was padded with two rows of pixels taken from the original (second) image. The procedure was repeated, but this time the padded window taken from the first image was shifted and compared to the corresponding window from the second image. The sign-corrected average of the two shift values (which usually were identical in magnitude and never differed by more than 2/40th of a pixel) was taken as the final displacement.

H. Calculation of tractions

To compute the tractions, the approach of Butler *et al.* was followed [17]. First, the Fourier transform of the displacement field was computed. Fourier components at wave vectors $\vec{k}=0$ were set to zero to eliminate translational artifacts. Second, the Fourier-transformed displacements were multiplied by $\tilde{K}(\vec{k})^{-1}$, where $\tilde{K}(\vec{k})$ denotes the Fourier transform of the Boussinesq solution to the Green's function that maps tractions to displacements on a half-infinite elastic space. Third, the inverse Fourier transform gave the tractions. Due to the low noise of 8 nm in the deformation field, there was no need for regularization [17,23]. Spurious tractions outside the cell boundaries were less than 0.3 Pa (rms).

III. RESULTS

Beads coated with the extracellular matrix protein fibronectin adhered firmly to the cells. Lateral forces of 10 nN that we imposed on the beads with magnetic tweezers were insufficient to disconnect the beads from the cell. The beads appeared tightly connected to the actin cytoskeleton, often with stress fibers extending from the bead (Fig. 2). This observation is in agreement with the notion that such beads do not merely attach to an already existing actin network but instead trigger integrin clustering, focal adhesion formation, and remodeling events within the cytoskeleton [24,25].

A. Mean-square displacement of CSK-bound beads

Despite their tight connection to the cytoskeleton, the beads moved spontaneously [Fig. 3(a)]. Over the course of our experiments (5–40 min), these movements were small compared to the cell size and are therefore thought to be unconstrained by distant cell boundaries [6].

The spontaneous bead motion was characterized using the MSD as a function of time lag Δt [Eq. (1)]. As reported previously, the MSDs of individual beads typically exhibited subdiffusive behavior for small Δt and superdiffusive behavior for large Δt ($\Delta t > 1$ s) [Fig. 3(b)] [4,9–11,26]. In particular, the MSD followed a power-law relationship over time [Eq. (2)] [Fig. 3(b)] [5,9–11,26]. Accordingly, the MSD was dominated by a constant term c for small Δt and by a superdiffusive term $D\,\Delta t^{\beta}$ for large Δt. The constant term c

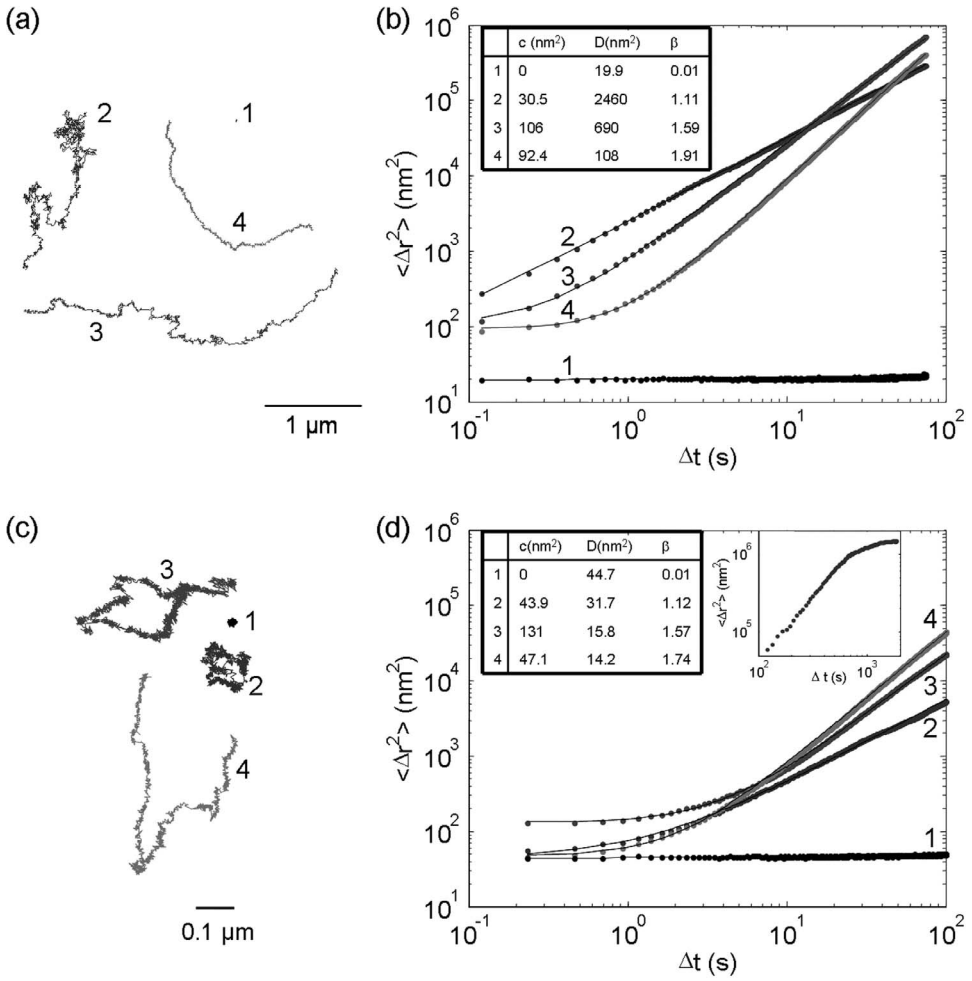

FIG. 3. Left: (a) Trajectories of the spontaneous movements of three representative 1-μm beads on MDA-MB-231 breast carcinoma cells (beads 2–4) and of a 1-μm bead immobilized on a rigid substrate (to quantify measurement noise, bead 1). (c) Trajectories of the spontaneous movements of three representative beads in the polyacrylamide gel beneath endothelial cells (beads 2–4) and of a bead in a gel without cells (to quantify measurement noise, bead 1). Right: The spontaneous motion of beads bound to cells (b) or to the gel (d) was quantified by the MSDs as function of time lag; the MSD increased with the time lag according to a power-law relationship [Eq. (2)]. The coefficient c, D, and β were estimated from a least-squares fit of Eq. (2) to the data (solid line). The inset of (d) shows the MSD with the expected plateau for a bead in the gel for large time lags.

reflects measurement noise ($\sim$25 nm^2 at 20$\times$magnification of the objective or 100 nm^2 at 10$\times$magnification) and fluctuations of the bead due to thermal or ATP-driven processes [9,27]. Note that the MSD due to thermal or ATP-driven fluctuations is not expected to exhibit a constant value, or plateau, at small Δt (except when the MSD of the beads falls below the noise floor) [9,10,14,28,29]. Nonetheless, we used Eq. (2) because it provided a robust and excellent fit to the MSD of individual beads over four decades in time, with the deviations between the fit and the measured MSD being only 3.4% on average and remaining below 10% in 98% of all beads.

B. Mean-square displacement of ECM-bound beads

When cells were plated onto elastic polyacrylamide gels, ongoing deformations of the gels were observed that appeared to be similar to the spontaneous motion of the beads bound to the cell surface. Gel deformations were quantified by tracking the position of fluorescent markers embedded in the gel. In what follows, the movements of both the beads on the cells and the beads in the gel were analyzed in the same way. Unless specified otherwise, measurements of beads on cells and beads in gels from multiple wells, cell isolations, and from different days were averaged.

The MSDs calculated from the gel displacements exhibited a behavior similar to that of the CSK-bound beads. Bead movements in the gel were subdiffusive for small Δt and superdiffusive for large Δt ($\Delta t > 5$ s). For large time lags ($\Delta t > 800$ s) the MSD exhibited a plateau of approximately 1.5 μm^2 [Fig. 3(d), inset]. Figures 3(c) and 3(d) show typical examples of trajectories and the corresponding MSD. The MSDs of beads in the gel were described by a power law according to Eq. (2). The deviations between the fit of Eq. (2) and the measured MSD were 2.8% on average and remained below 10% in 99% of the gel area.

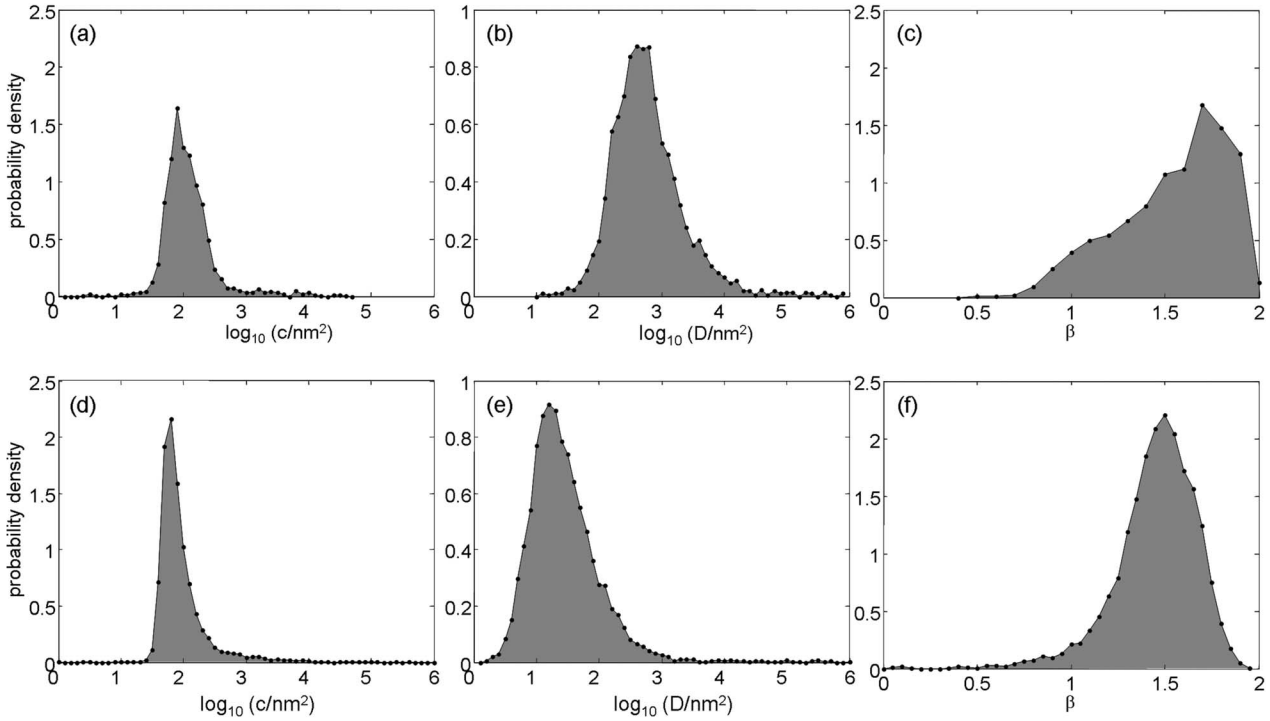

FIG. 4. Probability density distribution of the fit parameters of Eq. (2) to the MSD of 1-μm beads on Mewo skin carcinoma cells (n =2186) (top row) and beads in the polyacrylamide gel (n=9781) (bottom row). The plateau value c and the coefficient D display a nearly log-normal distribution, both on the cells (a),(b) and in the gel (d),(e). The power-law exponent β shows a left-skewed distribution both on the cells (c) and in the gel (f). For (a) and (d), only beads with $c>0$ were considered (91% of all beads on cells and 99.6% of all beads in the gel). Measurements from multiple wells and different days were averaged and performed separately for beads on cells and beads in the gel.

C. Comparison of CSK- and ECM-bound beads

Between individual CSK-bound beads or different gel regions, the parameters c and D were distributed over a wide range and exhibited approximately a log-normal distribution (Fig. 4). The short-time plateau of the MSD, c, was centered around 118 nm^2 for beads on cells and 92.4 nm^2 for beads in the gel, which are approximately the values one would expect from the measurement noise. The coefficient D had a geometric mean of 597 nm^2 for beads on cells and 27.8 nm^2 for beads in the gel. The geometric standard deviation of D was 3.7 for cells, 3.8 for the gel. The power-law exponent of the MSD, β, exhibited a left-skewed distribution with a mean of 1.54 for beads on cells (median 1.61) and 1.45 for beads in the gel (median 1.48), with a standard deviation of 0.29 for cells, 0.22 for the gel [Figs. 4(c) and 4(f)].

The wide, nearly log-normal distribution of D indicates that the geometric mean or the median, and not the arithmetic mean, should be used to calculate the average MSD over many beads or gel regions. To compare the average MSD of CSK- and ECM-bound beads, we first measured the gel deformations in fluorescent mode for 5 min and then switched to bright-field illumination to measure the movements of 4.5-μm beads bound to the same cells for another 5 min. The MSD of ECM-bound beads was right-shifted compared to CSK-bound beads, equivalent to a decrease in D, but both the power-law exponent β and the plateau c were similar (Fig. 5).

An examination of the MSD from individual beads or gel regions showed that MSDs with a high D (i.e., large MSD at short time scales) were usually associated with a low power-law exponent β (i.e., smaller MSD at long time scales) (Fig. 3). When β of individual beads was plotted against D, a relationship became apparent: beads with higher D tended towards lower β values (Fig. 6).

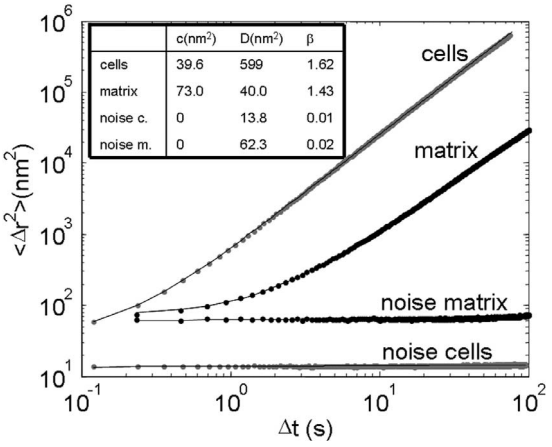

FIG. 5. MSD of 4.5-μm beads bound to endothelial cells (n =51) and of beads embedded in the matrix (n=961) within the same field of view (first measured in the gel, immediately afterwards on the cells) and of the corresponding noise measurement (noise cells, 4.5-μm bead immobilized on a rigid substrate; noise matrix, bead in the gel without cells). The coefficients c, D, and β (inset) were estimated from a least-squares fit of Eq. (2) to the data (solid line).

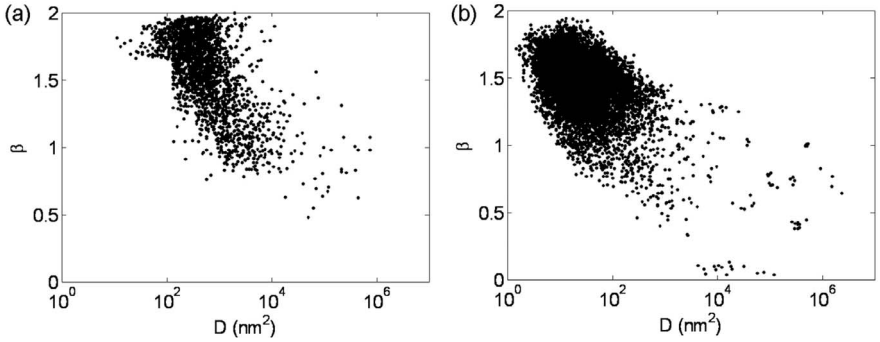

FIG. 6. Relationship between the power-law exponent β and coefficient D for 1-μm beads on Mewo skin carcinoma cells (a) and beads in the gel (b). Each data point represents one individual bead on a cell, or a 3.5×3.5 μm^2 region in the gel ($n=2186$ for cells, $n=9781$ in the gel). Beads with larger D tended to exhibit smaller exponents β ($r^2=0.4$ for cells, $r^2=0.28$ in the gel). Measurements from multiple wells and different days were averaged and performed separately for beads on cells and beads in the gel.

D. Persistence and superdiffusivity

The elongated shape of many bead trajectories (Fig. 3) indicated that their motion was not directionally random but showed persistence. To quantify directionality and persistence, the turning angle probability density of bead motion was computed. This method has been used to analyze chemotaxis in bacterial motility assays [30]. The probability density distribution of all turning angles within a bead trajectory was interpreted as follows: (i) For a bead motion that is directionally random, all turning angles between $-\pi$ and π would be equally likely. (ii) Persistent directional movement in which the direction in the previous time interval is correlated with the direction in the subsequent time interval would show as an increase in the probability of turning angles around zero. (iii) Antipersistent directional movement in which the direction in the previous time interval is anticorrelated with the direction in the subsequent time interval would show as an increase in the probability of turning angles around $\pm\pi$.

All three regimes—antipersistent, random, and persistent motion—were found in the bead trajectories. Which regime prevailed depended on the time lag Δt for which the direction of motion was calculated (see Methods). For $\Delta t<0.24$ s, the motion was antipersistent in 90% of all beads, became persistent on average at $\Delta t=0.7$ s, and was fully persistent for $\Delta t>1.32$ s in 90% of all beads. The turning angles computed from the displacements of the gel showed a similar behavior compared to CSK-bound beads, but the transition from antipersistent to persistent motion occurred at a longer time lag of $\Delta t=4.4$ s on average (Fig. 7).

To quantify persistent or antipersistent motion by a single number, for each bead or for each region in the gel an index of directionality p_d was computed as the difference between the probability of forward motion $\left(-\frac{\pi}{2}<\Delta\phi<\frac{\pi}{2}\right)$ and backward motion:

$$p_d = 2\left(\int_{-\pi/2}^{\pi/2} d\Delta\phi f_{\Delta\phi}\right) - 1, \tag{3}$$

where $f_{\Delta\phi}$ is the probability density of the turning angles [Fig. 7(a) and 7(c)]. The index of directionality p_d can take values between −1 and +1. A value of $p_d<0$ indicates antipersistent (anticorrelated) motion, $p_d=0$ indicates random motion, and $p_d>0$ indicates directed (persistent, correlated) motion. Using this index, we tested whether the transition between anticorrelated and directed motion was paralleled by a crossover from a subdiffusive to superdiffusive behavior in the MSD: For each bead the time lag $\Delta t_{pd=0}$ for which p_d crossed zero, and the time lag $\Delta t_{\beta=1}$ for which the MSD crossed from a subdiffusive to a superdiffusive behavior was computed (i.e., the time lag for which the MSD had a slope of unity). $\Delta t_{\beta=1}$ was computed from the fit of Eq. (2) to the MSD according to $\Delta t_{\beta=1}=\left(\frac{c}{D(\beta-1)}\right)^{1/\beta}$. $\Delta t_{\beta=1}$ tends towards infinity as β reaches unity. Therefore, beads that did not show a clear superdiffusive behavior ($\beta<1.1$, which was the case for 11% of all beads on cells and 6.0% of all beads in the gel) were excluded from this particular analysis. As expected, beads or gel regions for which the transition to directed motion occurred at large time lags tended to display a transition to superdiffusive behavior at similarly large time lags (Fig. 8).

Closer inspection of the bead trajectories (Fig. 3) showed that both the speed and directionality of bead and gel motion can change over time. To quantify such time fluctuations, a long time series (40 min for cells and 7 min in the gel) was subdivided into overlapping shorter time intervals of 1 min duration. For each 1-min time interval, Eq. (2) was fitted to the MSD. In addition, the directionality p_d was computed for each 1-min time interval at a time lag $\Delta t=3$ s for CSK-bound beads and at $\Delta t=7$ s for ECM-bound beads. These time lags were chosen to ensure that the persistent regime prevailed. When the power-law exponent of the MSD, β, and the index of directionality, p_d were plotted versus time, substantial fluctuations became evident (Fig. 9). The fluctuations of the power-law exponent and the directionality were highly correlated. The average correlation coefficient between fluctuations in β versus fluctuations in p_d was $r^2=0.59\pm0.24$ (mean±s.d., $n=2169$) for CSK-bound beads, and $r^2=0.41\pm0.19$ (mean±s.d., $n=961$) for ECM-bound beads.

E. Coupled motion of CSK- and ECM-bound beads

We next correlated the spatial fluctuations of each bead with the traction fluctuations everywhere on the gel. The

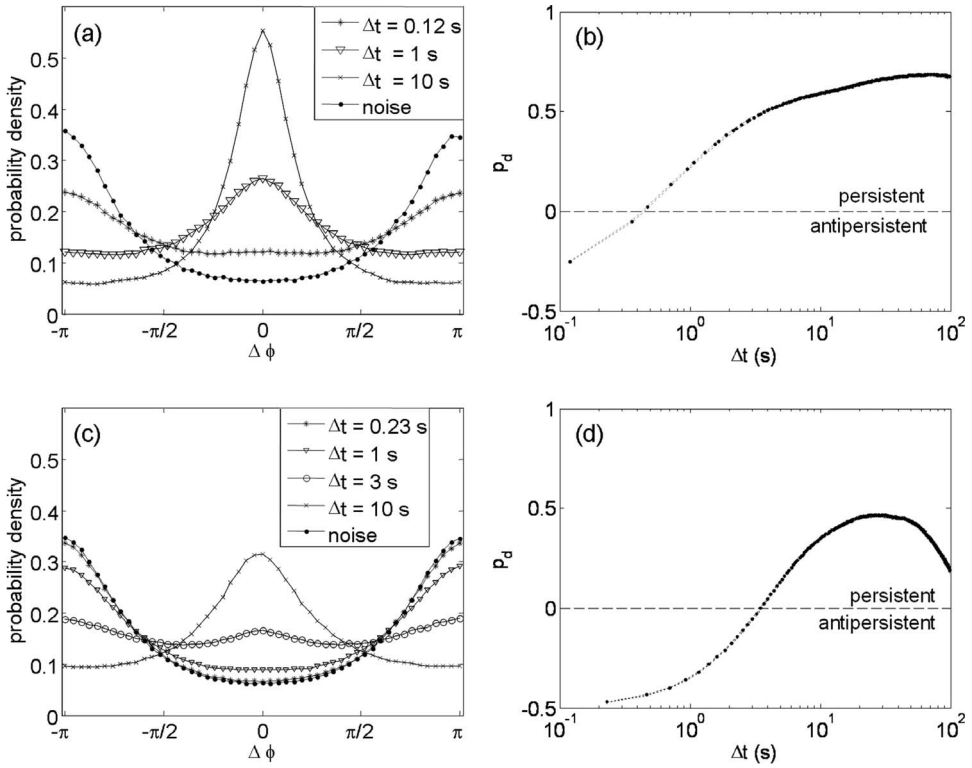

FIG. 7. Left: Distribution of the turning angle probability density of bead motion (a) (averaged over $n=2186$ 1-μm beads on Mewo skin carcinoma cells) and gel deformations (c) (averaged over $n=961$ regions in the polyacrylamide gel) for different time lags Δt. Turning angles around $-\pi$ or π were favored at small Δt (antipersistent motion), and turning angles around zero were favored at larger Δt (persistent motion). The behavior of beads immobilized on a rigid substrate or in a gel without cells (noise) was antipersistent regardless of the time lag Δt. Right: Directionality p_d [see Eq. (3)] versus time lag Δt for beads on cells (b) and in the gel (d). Measurements from multiple wells and different days were averaged and performed separately for beads on cells and beads in the gel.

bead movements and the matrix deformations were measured simultaneously over a period of 15 min. Tractions were computed from the matrix deformations as described above. For each bead-matrix pair, a correlation coefficient

$$C(i,j,k) = (\Delta\vec{T}_{ij} - \langle\Delta\vec{T}_{ij}\rangle) \cdot (\Delta\vec{r}_k - \langle\Delta\vec{r}_k\rangle) / \sqrt{\langle(\Delta\vec{T}_{ij} - \langle\Delta\vec{T}_{ij}\rangle)^2 \cdot (\Delta\vec{r}_k - \langle\Delta\vec{r}_k\rangle)^2}$$

was computed, where $\Delta\vec{T}_{ij}$ denotes the changes in traction for $\Delta t=60$ s at matrix positions i,j, $\Delta\vec{r}_k$ denotes the change in the position of bead k for $\Delta t=60$ s, and $\langle\cdots\rangle$ denotes the time average over a duration of 5, 10, or 15 min. We then determined for each bead-matrix pair whether the correlation between traction and spatial fluctuations was statistically significant. To be statistically significant, the correlation coefficient C had to exceed a significance threshold that was computed from a numerical simulation of uncorrelated traction fluctuations and bead fluctuations such that the probability p of a false positive correlation was $<8\times10^{-6}$ (corresponding <1 false positive correlation per image). The correlation thresholds were $C>0.94$ for a 5-min series, $C>0.69$ for a 10-min series, and $C>0.54$ for a 15-min series.

To visualize the data, each correlated bead-matrix pair was connected with a line (Fig. 10). Most beads were connected to multiple matrix locations, with distances spanning 38.5 μm on average. Incidentally, also numerous distant bead pairs on cells in a confluent monolayer, as well as distant bead pairs in the elastic substrate below the monolayer, displayed strong correlations (data not shown). With increasing measurement time, the number of correlated bead-matrix pairs decreased substantially. The possibility that this was an artifact caused by increasing numbers of false negative correlations could be ruled out: A numerical simulation of correlated tractions and bead fluctuations indicated that the number of bead-matrix pairs that exceeded the correlation thresholds listed above actually increased with increasing measurement time. Rather, our data are consistent with the notion that correlated tractions and bead fluctuations are transmitted via physical connections between the bead and the matrix, and that the number of connections that remain stable during the course of a measurement decreases over time.

IV. DISCUSSION

The principal findings of this report are these. Beads anchored to the CSK of adherent cells, as well as beads in an ECM onto which these cells adhere, show spontaneous motion. The MSD of both CSK-bound and ECM-bound beads displayed a transition from a subdiffusive to a superdiffusive behavior that was well described by a power law $\langle\Delta r^2(\Delta t)\rangle$

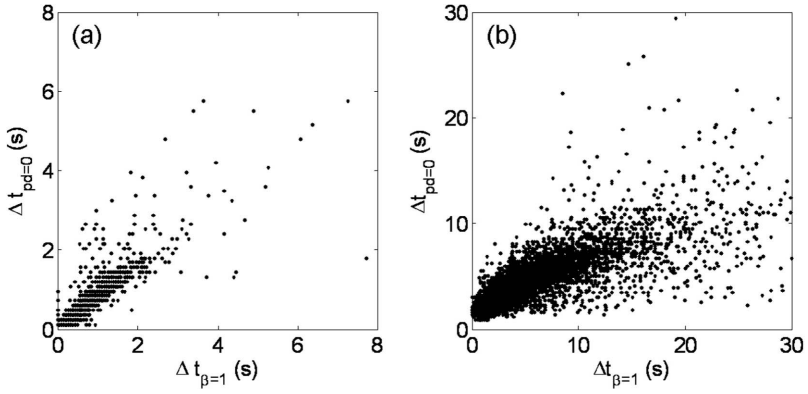

FIG. 8. The crossover time lag $\Delta t_{pd=0}$ from antipersistent to persistent motion vs crossover time lag $\Delta t_{\beta=1}$ from subdiffusive to superdiffusive behavior for 1-μm beads on Mewo skin carcinoma cells (a) and beads in the gel beneath endothelial cells (b). Each data point represents one bead or gel region ($n=1949$ on cells, $n=9171$ in the gel). The crossover time lags $\Delta t_{pd=0}$ and $\Delta t_{\beta=1}$ were highly correlated ($r^2=0.73$ for beads on cells, $r^2=0.37$ for beads in the gel). Measurements from multiple wells and different days were averaged and performed separately for beads on cells and beads in the gel.

$=c+D(\Delta t/t_0)^{\beta}$. The prefactor D exhibited a log-normal distribution and correlated with the power-law exponent β. Such behavior is reminiscent of the cell-to-cell distribution of power-law rheology parameters and the correlation between them [20,31,32], but whether and how power-law rheology and power-law superdiffusivity are linked is unclear. The power-law exponents β for both CSK-bound and ECM-bound beads were similar ($\beta \sim 1.5$). Both ECM- and CSK-bound beads displayed anticorrelated, antipersistent motion at short time lags ($\Delta t \sim 0.1$ s) and correlated, persistent motion at longer time lags ($\Delta t \sim 10$ s). Persistence and superdiffusivity of both CSK- and ECM-bound particles displayed large fluctuations over time. These fluctuations occurred synchronous; i.e., they were temporally correlated with each other. Moreover, the movements of CSK-bound beads were spatially correlated with forces exerted to the ECM.

A. Mechanisms of superdiffusivity and persistence

Our data on superdiffusive motion of beads coupled to the CSK of adherent cells are consistent with recent reports [5–7,9,10]. Superdiffusive bead motion cannot be explained by thermal forces alone and is not governed by the generalized Stokes-Einstein relationship [9,10]. Our data indicate that superdiffusivity and directional persistence are strongly coupled (Figs. 7–9).

1. Hopping mechanism

While it may appear obvious that superdiffusive behavior in the MSD is a direct consequence of directional persistence, there are alternative mechanisms that can account for superdiffusivity. One of them is a very wide distribution of step sizes (whereby a step is understood as the distance the bead has moved between two successive time points). In fact, this mechanism is commonly thought to be the main cause for superdiffusive behavior. Lau *et al.* proposed that directionally random motor hits act on beads bound to cells, whereby the power spectral density of those force fluctuations fall off with frequency ω according to $1/\omega^2$ [9]. Such a power spectrum of force hits would occasionally generate very large bead steps that become increasingly rare the larger their amplitude is. Similarly, Bursac *et al.* proposed a "stalling and hopping" motion of the beads [10]. Accordingly, they argued that the subdiffusive regime was associated with stalling and the superdiffusive regime with hopping. Moreover, they showed that the step size distribution for time lags $\Delta t \sim 1$ s had broad tails (which they interpret as hops), but for shorter or longer time lags, the step size distribution was more Gaussian.

Our data explain such apparent hops as a direct consequence of persistent motion: During periods of persistent motion during which the bead is steadily traveling in the same direction, it can cross far greater distances than a randomly diffusing bead. Another observation that argues against the existence of hopping motion is that large step sizes (i.e., hops) do not occur at the shortest time lags [10].

Our analysis of the turning angle distribution of bead motion clearly shows that the subdiffusive regime is associated with directionally anticorrelated (antipersistent) motion, and the superdiffusive regime is associated with directionally correlated (persistent) motion (Figs. 7–9). The transition between the subdiffusive and diffusive regimes occurred when the magnitude of the correlated motion exceeded that of the anticorrelated motion. Not coincidentally, the time lag of ~ 1 s that Bursac *et al.* reported to be associated with the largest deviation from a Gaussian step size distribution is nearly identical with the transition from anticorrelated to correlated behavior that we see in our data.

2. Caged motion

Anticorrelated and subdiffusive particle motion is reminiscent of caged motion of particles in a colloidal system, whereby the particle is confined, or trapped, by surrounding neighbors [10,33]. Caged motion would be in agreement with the notion that the rheological properties of cells and colloids alike arise from soft glassy dynamics [10,14,33]. Moreover, caged motion of small (250 nm) colloidal particles has been directly observed in entangled F-actin net-

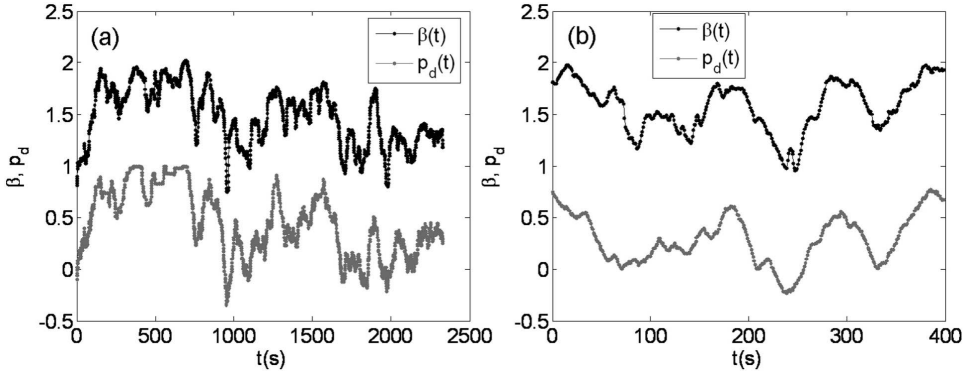

FIG. 9. Power-law exponent of the MSD, β, vs time (black) and the index of directionality p_d vs time (gray), for a representative bead on a MDA-MB-231 breast carcinoma cell (a) and in the gel beneath an endothelial cell (b). Over time, bead fluctuations undergo multiple transitions between random, undirected motion ($\beta \sim 1$, $p_d \sim 0$) and nearly ballistic motion ($\beta \sim 2$, $p_d \sim 1$). Fluctuations of β vs p_d were highly correlated with each other ($r^2=0.83$ for the bead on the cell, and $r^2=0.79$ for the bead in the gel).

works [34]. Whether caged dynamics is the mechanism responsible for anticorrelated, subdiffusive bead motion is questionable, however. First, there is no evidence in living cells that the CSK forms cages around large (≥ 1 μm) particles in which they can freely move. Rather, the beads appear tightly and directly coupled to the CSK via integrin adhesion receptors (Fig. 2) [12]. Second, optical and magnetic tweezers or twisting experiments reveal no initial slack of bead motion after the onset of force application [13,15,20,35]. Third, if caged motion were indeed the dominant source of bead movements at short time scales, larger beads would be expected to be more constrained by the cage boundaries [5]. Our data show that this is not the case, as we found no fundamental difference in the MSD at $\Delta t=0.12$ s for smaller (1 μm) and larger (4.5 μm) beads. We therefore considered caged motion to be an unlikely source for anticorrelated, subdiffusive bead motion and instead offer two alternative explanations.

3. Force fluctuations

a. Force fluctuations that lead to anticorrelated behavior. A trivial source of anticorrelated bead motion is measurement imprecision due to electronic noise, photon shot noise, mechanical vibrations, etc., that would give the impression that the beads move randomly around a fixed position [27]. Measurements of the MSD of beads immobilized on a plastic culture dish (noise measurements, Fig. 3) show that, at the shortest time lag, noise contributes substantially (18% for $20\times$ magnification and 71% for $10\times$ magnification) to the MSD of beads bound to cells. This noise is highly anticorrelated (Fig. 7). A second possible source of anticorrelated motion are force fluctuations within the viscoelastic CSK network, in particular within the stress fibers to which the beads are coupled (Fig. 2). Stress fibers are known to generate mechanical tension via the action of myosin motors [36,37]. Fluctuations in the tension generated by individual stress fibers (e.g., due to the cyclic activity of individual myosin motors within the fiber) would cause global, at short time scales predominantly elastic deformations within the CSK network to reestablish force balance [36,38,39]. Beads that are coupled to the CSK would then simply follow those elastic deformations and hence would move around an equilibrium position.

b. Force fluctuations that lead to correlated behavior. Force fluctuations in a viscoelastic, force-generating CSK network could also explain directed, superdiffusive bead motion: Stress fibers are known to be dynamic structures that undergo continuous formation, remodeling, and destruction [40]. A tension-generating stress fiber that is in the process of formation or destruction would cause the bead's equilibrium position to slowly drift until the stress fiber has been completely formed or destroyed. Of course, a single bead is connected to many tens of individual stress fibers (see Fig. 2), all with a different length, thickness, tension generation capability, and lifetime. As such, beads will be subject to force fluctuations at different magnitudes and time scales. In addition, dynamic restructuring of tension-carrying filaments that are not directly connected to the bead and that lead, for instance, to filopodia or lamellipodia formation, cell shape changes, and whole cell movements will be reported by correlated bead movements. However, previous studies have shown that within the time frame of our measurements (order of 5 min), such processes contribute only little to the total bead motion [10,41].

c. Measurement of force fluctuations. In this report, we set out to measure those force fluctuations that drive bead motion. We reasoned that all forces generated by the stress fibers must be counterbalanced by equal and opposite forces from the extracellular matrix, except for a small fraction of forces that are counterbalanced by the compression-bearing microtubule network within the cell [37,42]. The forces and force fluctuations that are transmitted to the extracellular matrix can be measured with traction microscopy. This method calculates the tractions exerted by the cell to their surroundings from the deformation field of an elastic polyacrylamide gel matrix onto which the cells adhere [19]. The deformation of the polyacrylamide gel is measured by tracking the displacements of fluorescent markers embedded at the gel surface. Elementary statistical properties of the cellular forces and force fluctuations, such as directional persistence, power spectral density, or mean-square displacement, can be deduced by analyzing the motion of the fluorescent markers in the gel matrix, without actually computing the forces them-

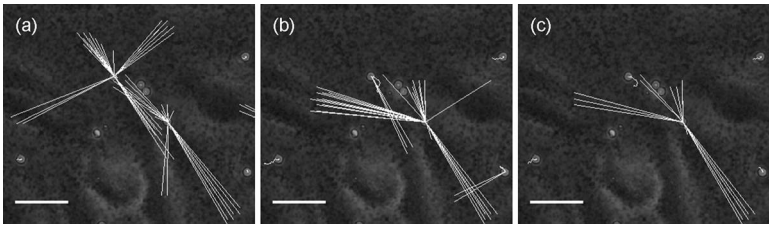

FIG. 10. Spatial correlation between the motion of CSK-bound beads on endothelial cells and the tractions in the gel matrix. The gel and the cells were measured in parallel, toggling between fluorescent mode and bright-field mode (switching time was 1 s). The number of correlated bead-matrix pairs (indicated by white lines) decreased over time [(a) after 5 min, (b) after 10 min, (c) after 15 min]. Bar 20 μm.

selves. This is because the displacement at any point $\vec{r}$ on the gel surface due to a point traction source at another point $\vec{r}'$ is, apart from the direction of the displacement and the direction of the traction, a function only of the difference $|\vec{r}-\vec{r}'|$ [17]. We therefore analyzed the MSD, power-law fit to the MSD [Eq. (2)], turning angle distribution $\Delta\phi(\Delta t)$, and directional persistence p_d for the beads in the gel in the very same way as we did for the beads on the cells.

d. Sources of matrix-anchored bead motion. While the mechanical environment of the beads bound to cells is highly complex (viscoelastic, glassy, nonlinear, heterogeneous, nonisotropic) and the details of the geometric coupling between the bead and the cell (bead internalization, cell thickness) are largely unknown, the mechanical environment of the matrix-bound beads is well characterized and simple: The matrix is a linear elastic, homogeneous, and isotropic material with a Young's modulus of 13 kPa. Its geometry is close to an infinite half-space [17,18]. This sets narrow limits on potential mechanisms that can be responsible for the kind of bead motion that is observed in the matrix. Caged dynamics, spontaneous rearrangements of the microconfiguration surrounding the beads, or other mechanisms that have been invoked to explain the diffusive behavior of particles in more complex systems can all be dismissed. Since thermal motion of the beads in the matrix is too small to be detected with our system, the only other sources of bead motion are measurement noise and force fluctuations arising from cell tractions. In our system, measurement noise dominated the motion of matrix-bound beads for time lags <4 s, but for larger time lags, the cell tractions deformed the matrix such that the motion of matrix-bound beads was superdiffusive and directionally persistent.

B. Coupled motion of CSK- and matrix-bound beads

We found strikingly similar superdiffusive and directionally persistent behavior in the motion of CSK-bound and matrix-bound beads (Figs. 3, 5, 7, 9, and 10). This observation supports the physical picture developed above: The motion of CSK-bound beads follows the CSK deformations caused by stress fluctuations that are generated by the CSK network itself, in particular by the stress fibers. If that is the case, we reasoned that the tractions exerted by the stress fibers to the elastic extracellular matrix (the polyacrylamide gel) should occur synchronous with the motion of CSK-bound beads. To test this hypothesis, we simultaneously measured the motion of CSK-bound beads and the cell tractions over a period of 15 min and computed the correlation between the displacement fluctuations and the traction fluctuations. In agreement with our hypothesis, the displacement fluctuations of most beads correlated significantly with traction fluctuations at multiple matrix positions (Fig. 10). Interestingly, the number of correlated bead-matrix pairs decreased with increasing duration of the time frame over which the correlation analysis was performed (Fig. 10). We interpret the loss of correlated bead-matrix pairs over time with the ongoing disassembly of stress fibers that form a connection between the bead and the matrix. There were two notable differences between the motion of CSK-bound beads and matrix-bound beads, however. First, the displacements of matrix-bound beads were on average $\sim$10-fold smaller than those of CSK-bound beads, and the MSD curves were accordingly shifted (Fig. 3). This is explained by the fact that the magnitude of the matrix deformations depends linearly on the matrix stiffness. The matrix deformations increase with decreasing matrix stiffness as long as the force-generating capability of the cell is not degraded due to a matrix that is too soft [19,43]. Our choice of a matrix stiffness of 13 kPa was a compromise between sufficient resolution of the displacement field (requiring a low stiffness) and high cell tractions (requiring a high stiffness).

A second difference between the motion of the CSK-bound and matrix-bound beads was that the matrix displacements were not unbounded during our measurement period, as can be seen from the plateau in the MSD after $\sim$800 s [Fig. 3(d), inset]. This is due to the fact that the maximum matrix deformations are set by the maximum tractions the cell can generate. A consequence of an upper bound for the matrix deformations is that directional persistence cannot be maintained for prolonged periods in time. We found that the directional persistence p_d in the motion of matrix-bound beads began to decrease for time lags larger than 30 s (Fig. 7).

C. Conclusion

In an accompanying theoretical paper [44], we suggest that the transition from subdiffusive to superdiffusive behavior in the MSD and the transition from antipersistent to persistent bead motion is caused by the crossover between two distinct force regimes: At short time lags, the bead is diffusing due to random force fluctuations within the (predominantly elastic) medium of the cell. At longer time lags, the

bead is actively transported by persistent forces. The resulting bead trajectories would then be reminiscent of a particle diffusing in a slowly drifting potential well.

A biologically plausible realization of this generic picture is a CSK-bound bead in a network of ATP-powered actomyosin stress fibers. The stress fibers form an elastic potential well at short time lags that suppresses bead diffusion (subdiffusive regime). At longer time lags, the stress fibers run through a remodeling life cycle and thus increase or decrease their tension as they are assembled or disassembled. These tension changes are directionally persistent and lead to superdiffusive bead motion. Despite its simplicity, this biologically plausible model of a tensed and continuously remodeling cytoskeletal network accounts quantitatively for our data.

ACKNOWLEDGMENTS

The authors are indebted to J.P. Butler for suggesting the analysis of the turning angle distribution of the bead trajectories, B. Reischl for help with cell culture, S. Greiner for rheometer measurements, and J. Smith for critical comments. This work was supported by the Deutsche Forschungsgemeinschaft, the Deutsche Krebshilfe, and the National Institutes of Health, Grants Nos. MA 534/20-4, 107384, and HL65960.

[1] Y. Marcy, J. Prost, M. F. Carlier, and C. Sykes, Proc. Natl. Acad. Sci. U.S.A. **101**, 5992 (2004).
[2] N. Watanabe and T. J. Mitchison, Science **295**, 1083 (2002).
[3] P. Vallotton, A. Ponti, C. M. Waterman-Storer, E. D. Salmon, and G. Danuser, Biophys. J. **85**, 1289 (2003).
[4] C. E. Schmidt, A. F. Horwitz, D. A. Lauffenburger, and M. P. Sheetz, J. Cell Biol. **123**, 977 (1993).
[5] A. Caspi, R. Granek, and M. Elbaum, Phys. Rev. E **66**, 011916 (2002).
[6] S. S. An, B. Fabry, M. Mellema, P. Bursac, W. T. Gerthoffer, U. S. Kayyali, M. Gaestel, S. S. Shore, and J. J. Fredberg, J. Appl. Physiol. **96**, 1701 (2004).
[7] A. Caspi, R. Granek, and M. Elbaum, Phys. Rev. Lett. **85**, 5655 (2000).
[8] M. P. Sheetz, D. P. Felsenfeld, and C. G. Galbraith, Trends Cell Biol. **8**, 51 (1998).
[9] A. W. C. Lau, B. D. Hoffman, A. Davies, J. C. Crocker, and T. C. Lubensky, Phys. Rev. Lett. **91**, 198101 (2003).
[10] P. Bursac, G. Lenormand, B. Fabry, M. Oliver, D. A. Weitz, V. Viasnoff, J. P. Butler, and J. J. Fredberg, Nat. Mater. **4**, 557 (2005).
[11] D. Margineantu, R. A. Capaldi, and A. H. Marcus, Biophys. J. **79**, 1833 (2000).
[12] N. Wang, J. P. Butler, and D. E. Ingber, Science **260**, 1124 (1993).
[13] A. R. Bausch, F. Ziemann, A. A. Boulbitch, K. Jacobson, and E. Sackmann, Biophys. J. **75**, 2038 (1998).
[14] B. Fabry, G. N. Maksym, J. P. Butler, M. Glogauer, D. Navajas, and J. J. Fredberg, Phys. Rev. Lett. **87**, 148102 (2001).
[15] M. Balland, A. Richert, and F. Gallet, Eur. Biophys. J. **34**, 255 (2005).
[16] B. D. Hoffman, G. Massiera, K. M. Van Citters, and J. C. Crocker, Proc. Natl. Acad. Sci. U.S.A. **103**, 10259 (2006).
[17] J. P. Butler, I. M. Tolic-Norrelykke, B. Fabry, and J. J. Fredberg, Am. J. Physiol. **282**, C595 (2002).
[18] M. Dembo and Y. L. Wang, Biophys. J. **76**, 2307 (1999).
[19] R. J. Pelham, Jr. and Y. Wang, Proc. Natl. Acad. Sci. U.S.A. **94**, 13661 (1997).
[20] B. Fabry, G. N. Maksym, S. A. Shore, P. E. Moore, R. A. Panettieri, Jr., J. P. Butler, and J. J. Fredberg, J. Appl. Physiol. **91**, 986 (2001).
[21] O. Müller, H. E. Gaub, and E. Sackmann, Macromolecules **24**, 3111 (1991).
[22] S. Hu, J. Chen, B. Fabry, Y. Numaguchi, A. Gouldstone, D. E. Ingber, J. J. Fredberg, J. P. Butler, and N. Wang, Am. J. Physiol.: Cell Physiol. **285**, C1082 (2003).
[23] U. S. Schwarz, N. Q. Balaban, D. Riveline, A. Bershadsky, B. Geiger, and S. A. Safran, Biophys. J. **83**, 1380 (2002).
[24] G. Plopper and D. E. Ingber, Biochem. Biophys. Res. Commun. **193**, 571 (1993).
[25] L. Deng, N. J. Fairbank, B. Fabry, P. G. Smith, and G. N. Maksym, Am. J. Physiol.: Cell Physiol. **287**, C440 (2004).
[26] S. S. An, R. E. Laudadio, J. Lai, R. A. Rogers, and J. J. Fredberg, Am. J. Physiol.: Cell Physiol. **283**, C792 (2002).
[27] T. Savin and P. S. Doyle, Biophys. J. **88**, 623 (2005).
[28] T. G. Mason and D. A. Weitz, Phys. Rev. Lett. **74**, 1250 (1995).
[29] J. C. Crocker, M. T. Valentine, E. R. Weeks, T. Gisler, P. D. Kaplan, A. G. Yodh, and D. A. Weitz, Phys. Rev. Lett. **85**, 888 (2000).
[30] H. C. Berg and D. A. Brown, Nature (London) **239**, 500 (1972).
[31] B. Fabry, G. N. Maksym, J. P. Butler, M. Glogauer, D. Navajas, N. A. Taback, E. J. Millet, and J. J. Fredberg, Phys. Rev. E **68**, 041914 (2003).
[32] M. Balland, N. Desprat, D. Icard, S. Fereol, A. Asnacios, J. Browaeys, S. Henon, and F. Gallet, Phys. Rev. E **74**, 021911 (2006).
[33] E. R. Weeks, J. C. Crocker, A. C. Levitt, A. Schofield, and D. A. Weitz, Science **287**, 627 (2000).
[34] I. Y. Wong, M. L. Gardel, D. R. Reichman, E. R. Weeks, M. T. Valentine, A. R. Bausch, and D. A. Weitz, Phys. Rev. Lett. **92**, 178101 (2004).
[35] G. Lenormand, E. Millet, B. Fabry, J. P. Butler, and J. J. Fredberg, J. R. Soc., Interface **1**, 91 (2004).
[36] S. Kumar, I. Z. Maxwell, A. Heisterkamp, T. R. Polte, T. P. Lele, M. Salanga, E. Mazur, and D. E. Ingber, Biophys. J. **90**, 3762 (2006).
[37] N. Wang, I. M. Tolic-Norrelykke, J. Chen, S. M. Mijailovich, J. P. Butler, J. J. Fredberg, and D. Stamenovic, Am. J. Physiol.: Cell Physiol. **282**, C606 (2002).
[38] S. Deguchi, T. Ohashi, and M. Sato, J. Biomech. **38**, 1751 (2005).
[39] D. Stamenovic, B. Suki, B. Fabry, N. Wang, and J. J. Fredberg,

J. Appl. Physiol. **96**, 1600 (2004).
[40] K. K. Parker, A. L. Brock, C. Brangwynne, R. J. Mannix, N. Wang, E. Ostuni, N. A. Geisse, J. C. Adams, G. M. Whitesides, and D. E. Ingber, FASEB J. **16**, 1195 (2002).
[41] P. Bursac, B. Fabry, X. Trepat, G. Lenormand, J. P. Butler, N. Wang, J. J. Fredberg, and S. S. An, Biochem. Biophys. Res. Commun. (to be published).
[42] D. Stamenovic, S. M. Mijailovich, I. M. Tolic-Norrelykke, J. Chen, and N. Wang, Am. J. Physiol.: Cell Physiol. **282**, C617 (2002).
[43] D. E. Discher, P. Janmey, and Y. L. Wang, Science **310**, 1139 (2005).
[44] C. Metzner, C. Raupach, D. Paranhos Zitterbart, and B. Fabry (unpublished).